Design of a Nonlinear Damping Control Scheme for Nanopositioning

Marialena Vagia, Arnfinn A. Eielsen, J. Tommy Gravdahl and Kristin Y. Pettersen

Abstract— **The application of a nonlinear control law for vibration damping on a typical nanopositioning system is investigated. The nonlinear control law is an augmentation of the linear integral force feedback scheme, where the constant gain used in integral force feedback, is replaced by a passive nonlinear operator. The nonlinear control law improves the performance of integral force feedback as it provides more rapid suppression of large disturbances, while maintaining low noise sensitivity. $\mathcal{L}_2$-stability for the control law is established. Experimental results are presented, showing improved performance when applying the nonlinear augmentation of the integral force feedback scheme, compared to the original linear integral force feedback scheme.**

I. Introduction

Nanoscience and nanotechnology have experienced substantial growth in recent decades, contributing to numerous areas such as biology, chemistry, materials science, and physics [1]. A key enabling technology for nanoscience and nanotechnology is scanning probe microscopy [2], [3], as scanning probe microscopy can be used for both manipulation [4] and interrogation [5] at the nanometer scale.

Scanning probe microscopy requires one or more positioners to physically position the probe in space. As such, scanning probe microscopy requires high performance motion control. The motion can be generated using e.g. piezoelectric actuators [6], [7], electrostatic comb drives [8], or voice coil actuators [9], [10]. However, many positioner designs feature high stiffness materials and little structural damping. Thus, the mechanical structures of such devices have lightly damped vibration modes which limit the usable bandwidth, since reference signals with high frequency components will excite the vibration modes, which results in non accurate positioning. In addition, the device is affected by environmental disturbances, such as sound and floor vibrations. Depending on the actuator, a positioner might exhibit various non-linear behavior as well.

For known signals, the effect of mechanical vibrations in these systems can be reduced using feed-forward techniques [11]. However, feedback control may be necessary in order to reduce the sensitivity to uncertainty and unknown disturbances. In order to control lightly damped vibrational modes in active structures, several control schemes that introduce damping have been developed, such as positive position feedback [12], integral force feedback [13], passive shunt-damping [14], resonant control [15] and integral resonant control [16]. With regards to nanopositioning applications, positive position feedback and resonant control has been applied in [17], integral force feedback in [18], passive shunt-damping in [19], [20], and integral resonant control in [21]. These control schemes tend to be simple to implement and robust towards plant uncertainty and nonlinearities.

All these control schemes are very effective in introducing damping and reducing the sensitivity of the systems they are applied to. However, since they are linear control laws, there are general limitations to the achievable performance [22]. Additional improvement in performance can be obtained using nonlinear control laws.

In this paper, the nonlinear control law for vibration damping presented in [23] is applied to a nanopositioning device. The nonlinear control law in an augmentation of the integral force feedback (IFF) scheme [13]. When applying IFF, the output of a piezoelectric force transducer is integrated, multiplied with a gain constant, and applied to a co-located actuator. The augmented nonlinear control law replaces the gain constant with a passive nonlinear operator which includes a second-order term. The nonlinear control law improves the performance of integral force feedback as it provides more rapid suppression of large disturbances, while maintaining low noise sensitivity, since the second-order term only provides high gain for large error signals. The stability properties of the closed loop system can be established using the theory of passivity [24].

The control law has been implemented on a nanopositioning device. The aim of the control law is not to achieve reference trajectory tracking, but to reject unknown exogenous disturbances. Experimental results are presented, which confirm that the nonlinear control law provides improved performance compared to an optimally tuned linear IFF scheme.

The paper is organized as follows: In Section II the nanopositioning system and the mathematical model is presented. Section III presents integral force feedback and then nonlinear control law, together with results establishing $\mathcal{L}_2$-stability. Experimental results are presented in Section IV. In Section VI conclusions are drawn.

II. System Description and Modeling

A. Description of the Experimental System

The experimental set-up consists of a dSPACE DS1103 hardware-in-the-loop (HIL) system, an ADE 6810 capacitive gauge, an ADE 6501 capacitive probe from ADE Technologies, a Piezodrive PDL200 voltage amplifier, two SIM 965 programmable filters from Stanford Research Systems, and the custom-made long-range serial-kinematic nanopositioner

This paper is partially supported by KMB project NextGenRob, Next Generation Robotics for Norwegian Industry.
The authors are with the Dept. of Engineering Cybernetics, Norwegian Univ. of Science and Technology, Trondheim, Norway, Corresponding author email: marialev@itk.ntnu.no

shown in Fig. 1. The nanopositioner is fitted with a Noliac SCMAP07-H10 actuator, where one of the stack elements is used as a force transducer. The transducer charge is measured using a simple charge conditioning amplifiers employing a Burr-Brown OPA2111. The voltage amplifier with the capacitive load of the actuator, has a first-order response and a bandwidth around 40 kHz. With the DS1103 board, a sampling frequency of $f_s = 125$ kHz was obtained. For numerical integration, a third-order Runge-Kutta scheme was used. Two second-order Butterworth filters with a cut-off frequency of 40 kHz were used as anti-aliasing and reconstruction filters.

The experimental set-up includes the custom-made long-range serial-kinematic nanopositioner shown in Fig. 1. The serial-kinematic motion mechanism is designed to make the first vibration mode dominant and to occur in the actuation direction (piston mode). More details on the design of this stage can be found in [25].

The displacement is generated using a piezoelectric actuator. Such actuators generate a force proportional to an applied voltage [26]. The applied external force from the piezoelectric actuator f_a (N) can be expressed as

$$f_a = e_a u \ , \tag{1}$$

where e_a (N V^{-1} = C N^{-1}) is the effective gain of the piezoelectric actuator from voltage to force, and u (V) is the applied voltage.

The dynamics due to an applied voltage u for a point d (m) on the flexible structure, as observed by a co-located sensor, is adequately described by the following lumped parameter, truncated linear model [27],

$$G_d(s) = e_a \frac{d}{f_a}(s) \approx \sum_{i=1}^{n_d} \frac{\beta_i}{s^2 + 2\zeta_i \omega_i s + {\omega_i}^2} + D_r \tag{2}$$

where n_d is the number of vibration modes included. Here, $\{\beta_i\}$ (m s^{-2} V^{-1}) are the control gains, $\{\zeta_i\}$ are the damping coefficients for each mode, and $\{\omega_i\}$ (rad s^{-1}) are the natural frequencies for the modes. The term D_r (m V^{-1}) is the residual mode, which is an approximation of the non-modeled higher frequency modes, and can be included to improve prediction of zero-locations. The addition of D_r produces a model that is not strictly proper, but as the instrumentation, such as the amplifier and sensors, have limited bandwidth, D_r can be considered equal to zero for this system.

The integral force feedback scheme utilizes a co-located piezoelectric force transducer. The force transducer generates a charge, depending on the applied force. The current or charge produced by the force transducer is typically converted to a voltage signal using a simple op-amp circuit with a high input impedance. The output voltage from such a sensor when measuring the charge, can be found to be [18], [27]

$$v_f = k_s(k_f u - d) \ ,$$

where d is the displacement of the mechanical structure, u is the applied voltage to the actuator, k_f (m V^{-1}) is the gain of the feed-through term, and k_s (V m^{-1}) is the sensor gain. The transfer-function from applied voltage u_a to measured sensor voltage v_f can therefore be found as

$$G_f(s) = \frac{v_f}{u}(s) = k_s(k_f - G_d(s)) \ . \tag{3}$$

In order to identify the parameters in (2) and (3), the frequency responses for the displacement and force were recorded using an SR780 Dynamic Signal Analyzer from Stanford Research Systems using a 100-mV RMS bandwidth-limited white noise excitation. The models were fitted to the procured data using the MATLAB System Identification Toolbox and Optimization Toolbox. The responses for $G_d(s)$, and $G_f(s)$ are displayed in Figs. 2a and 2b, respectively. The identified parameter values are presented in Tab. I. For the displacement model (2), only the dominant vibration mode is included, i.e. $n_d = 1$. The dominant piston mode occurs at 1680 Hz.

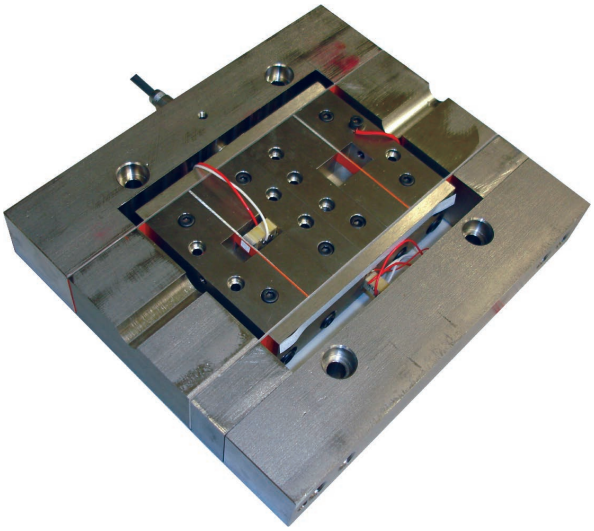

Fig. 1: Custom flexure-guided nanopositioning stage.

TABLE I: Identified model parameters.

Displacement model (2)		
β_1	$2.00 \cdot 10^6$	μm s^{-2} V^{-1}
ζ_1	0.0196	
ω_1	$2\pi \cdot 1680$	rad s^{-1}
Force model (3)		
k_s	0.00197	V μm^{-1}
k_f	0.0253	μm V^{-1}

III. Control Schemes

A. Integral Force Feedback

Integral force feedback (IFF) was introduced in [13], and has successfully been applied to a nanopositioning device in [18]. An advantage of using this scheme, is that a piezoelectric force transducer typically has an extremely low noise density, compared to many other sensors [18]. The control law is also simple to tune and implement, as provides damping for several vibration modes simultaneously.

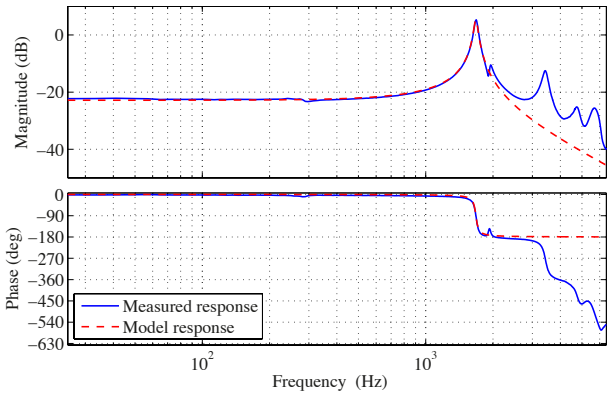

(a) Displacement.

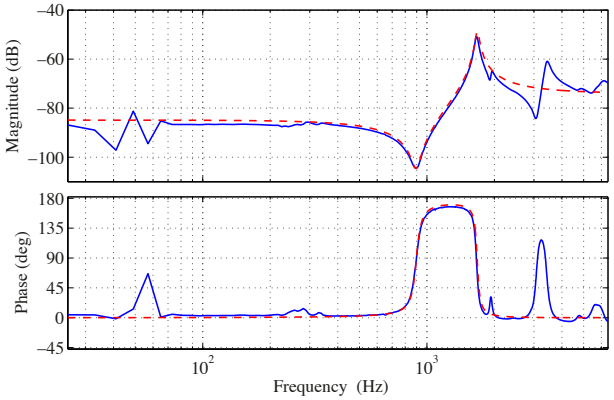

(b) Force transducer.

Fig. 2: Frequency responses; measured and using the models.

Assuming sensor-actuator co-location, it provides robust $\mathcal{L}_2$-stability.

The basic implementation of the control scheme is shown in Fig. 3a. Here

$$\Phi = k_2$$

and the IFF control scheme is therefore equivalent of the integral control law on the form

$$C(s) = \frac{k_2}{s}\,, \tag{4}$$

where k_2 is the control law gain.

The methodology for optimally tuning the gain k_2 is elaborately explained in [18], [28]. Ignoring the damping, $\zeta_1 = 0$, and assuming that $\pm j\omega_1$ are the poles and $\pm jz_1$ are the zeros of $G_f(s)$, then, if $z_1 > \omega_1/3$, the maximum achievable damping using IFF is

$$\zeta_1^{\max} = \frac{\omega_1 - z_1}{2z_1}\,,$$

which occurs when

$$k_2 = \omega_1\sqrt{\frac{\omega_1}{z_1}}\frac{1}{k_f k_s}\,. \tag{5}$$

For the system at hand, this results in $k_2 = 7.2 \cdot 10^7$. When not ignoring the damping, the optimal value is slightly

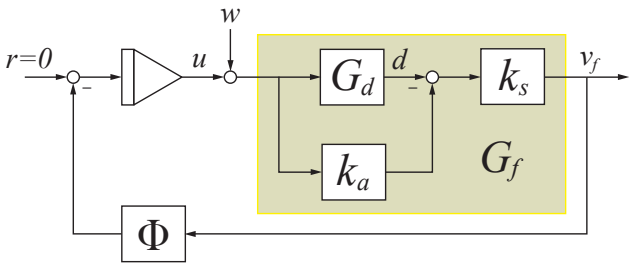

(a) Integral force feedback.

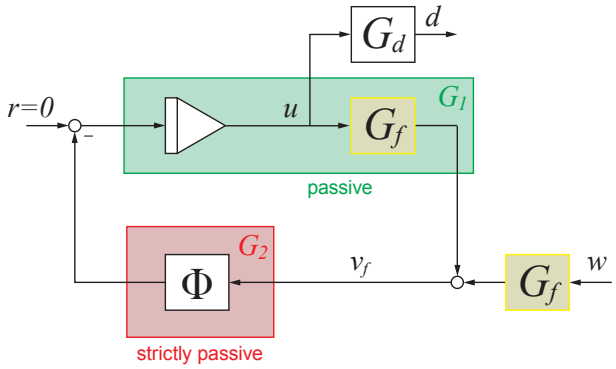

(b) Equivalent representation.

Fig. 3: Block diagrams for closed-loop system.

different. Maximum damping is achieved where the root locus intersects a line radiating from the origin, and this is simply found by plotting the root locus for $C(s) \cdot G_f(s)$, as has been done in Fig. 4. In this case $k_2 = 7.4 \cdot 10^7$ is found to be optimal, and is the value used in the experiments.

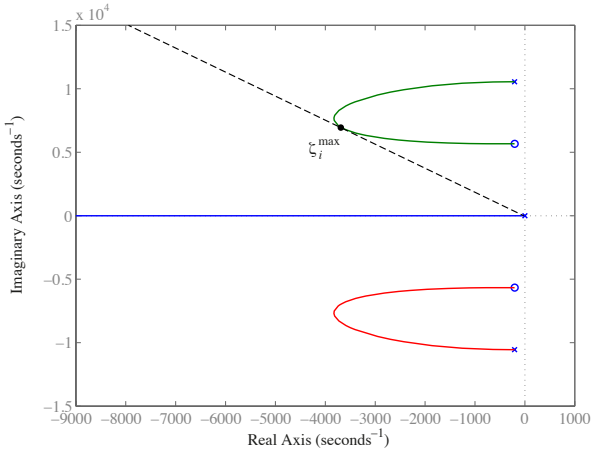

Fig. 4: Root locus of $1/s \cdot G_f(s)$.

B. Nonlinear Control Scheme

Linear control laws in general have limitations to the achievable performance [22]. For a single-input-single-output system, this is perhaps most noticeable from the limitations imposed by the Bode sensitivity integral [29]. For the IFF scheme, performance depends on the tuning for the gain

k_2 in (4). There is one optimal value for the gain k_2 that provide maximum damping. Choosing other values for k_2 results in either a larger overshoot, a longer convergence envelope, or both. In order to improve the performance of the IFF scheme, a nonlinear augmentation was proposed in [23]. Here, a gain proportional to the force measurement is added to the constant gain k_2. Thus, with reference to Fig. 3a,

$$\Phi = K$$

where

$$K = \text{sat}(k_1|v_f|, L) + k_2, \quad L, k_1, k_2 > 0 \tag{6}$$

and

$$\text{sat}(x, L) = \begin{cases} x, & |x| < L \\ L\,\text{sgn}(x), & |x| \geq L \end{cases} .$$

In order to establish $\mathcal{L}_2$-stability, the closed-loop system in Fig. 3a is put on the equivalent form shown in Fig. 3b. Firstly, the nonlinear gain is examined. The inner product on the extended $\mathcal{L}_2$-space of the input v_f to the output of the operator, or sector nonlinearity,

$$\Phi(v_f) = (\text{sat}(k_1|v_f|, L) + k_2)\, v_f$$

is

$$\begin{aligned} \langle \Phi(v_f)|v_f\rangle_T = \int_0^T \Phi(v_f) v_f \,\mathrm{d}t = \\ \int_0^T (\text{sat}(k_1|v_f|, L) + k_2) {v_f}^2 \,\mathrm{d}t \geq \\ \int_0^T k_2 {v_f}^2 \,\mathrm{d}t = k_2 ||v_f||_T^2 , \end{aligned} \tag{7}$$

which satisfies the requirements for being strictly passive according to Theorem 1 in the Appendix. In addition, the operator $\Phi(v_f)$ has a finite gain, i.e.,

$$\begin{aligned} \|\Phi(v_f)\|_T = \left(\int_0^T \Phi(v_f)^2 \,\mathrm{d}t \right)^{1/2} = \\ \left(\int_0^T (\text{sat}(k_1|v_f|, K) + k_2)^2) v_f^2 \,\mathrm{d}t \right)^{1/2} \leq \\ \left(\int_0^T (K + k_2)^2 v_f^2 \,\mathrm{d}t \right)^{1/2} = (K + k_2)\|v_f\|_T . \end{aligned} \tag{8}$$

Next, consider the transfer function

$$\frac{1}{s} \cdot G_f(s) = \frac{1}{s} k_s \left(k_f - \sum_{i=1}^{n_d} \frac{\beta_i}{s^2 + 2\zeta_i\omega_i s + {\omega_i}^2} - D_r \right)$$

for which the Fourier transform is

$$\begin{aligned} G_1(j\omega) = \frac{1}{j\omega} \cdot G_f(j\omega) = \\ k_s \left(\sum_{i=1}^{n_d} \frac{\beta_i \left(2\zeta_i\omega_i\omega^2 + j({\omega_i}^2\omega - \omega^3) \right)}{(2\zeta_i\omega_i\omega^2)^2 + ({\omega_i}^2\omega - \omega^3)^2} - j\frac{k_f - D_r}{\omega} \right) , \end{aligned}$$

thus

$$\begin{aligned} \mathbf{Re}\,[G_1(j\omega)] = \\ k_s \left(\sum_{i=1}^{n_d} \frac{2\zeta_i\omega_i\beta_i\omega^2}{(2\zeta_i\omega_i\omega^2)^2 + ({\omega_i}^2\omega - \omega^3)^2} \right) \geq 0 \;\forall\; \omega \in \mathbb{R} , \end{aligned} \tag{9}$$

and given Theorem 2 in the Appendix, it can be seen that the mapping $u \mapsto \int_0^t v_f(t)$, described by $G_1(j\omega)$, is passive.

Now, (7) and (8) establishes that $\Phi(v_f)$ is a strictly passive mapping with finite gain, and (9) establishes that $\frac{1}{s}G_f(s)$ is passive, the operator $G_f(s)$ is also exponentially stable, thus the closed-loop system is $\mathcal{L}_2$-stable with exogenous disturbances w according to Theorem 3 in the Appendix.

IV. Experimental Results

Experiments were carried out applying the linear control law and the nonlinear control law on the system described in Section II. A diagram for the implementation of the control laws is shown in Fig. 5. Here $W_o(s)$ represents the dynamics due to the reconstruction filter and the voltage amplifier, and $W_i(s)$ the dynamics due to the capacitive sensor gauge and anti-aliasing filter. As the charge measurement had a bias component, a second-order high-pass Butteworth filter with a cut-off frequency of 1 Hz was introduced, represented by $W_{hp}(s)$.

For the linear control law, Φ was the to the constant gain as in (5), and in the case of the nonlinear control law, Φ was defined as in (6). In order to avoid integral windup and amplification of low-frequency noise from the charge amplifier, a limited integrator,

$$C(s) = \frac{s}{s + \omega_{li}} \cdot \frac{1}{s} , \tag{10}$$

was used. The cut-off frequency ω_{li} was set to 50 Hz.

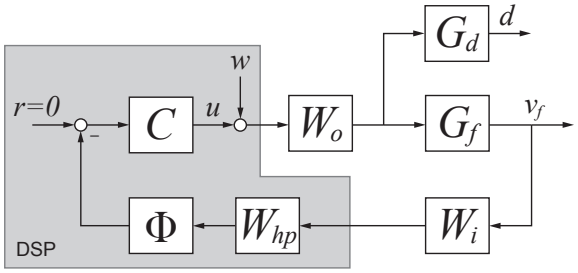

Fig. 5: Experimental implementation.

In order to assess the performance of the linear control law and the nonlinear control law, a disturbance signal w was generated as a 5 Hz square-wave with an amplitude of 6 V which was applied to the piezoelectric actuator, and the resulting displacement was measured.

The tuning of the linear control law used, was as presented in Section III and Fig. 4, i.e., $k_2 = 7.4 \cdot 10^7$. As the nonlinear control law is an augmentation of the linear control law, with the addition of a second-order damping term with gain k_1, the gain for the linear component k_2 was kept at the same value. The tuning for gain k_1 was simply done by increasing it until

the system went unstable, and then reducing it somewhat. The value used for the experiments was $k_1 = 2.0 \cdot 10^{12}$. The main limiting factor for the gain k_1 appears to be the low-pass characteristic dynamics of the instrumentation, as reducing the cut-off frequency of the programmable low-pass filters also reduced the maximum gain before instability. The higher the value of k_1, the more effective the nonlinear control law appears to be.

Time-series of the responses from the displacement sensor and the force transducer when applying the square-wave excitation signal as a disturbance are presented in Figs. 6 and 7, respectively. The responses when using the linear and the nonlinear control laws are shown. A power spectral density estimate for the displacement measurement is shown in Fig. 8. Here the plot also includes the results from when operating the system in open-loop.

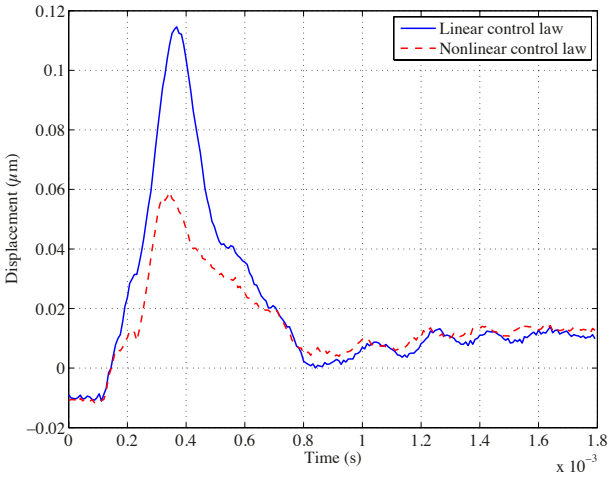

Fig. 6: Measured displacement for the linear and nonlinear control law.

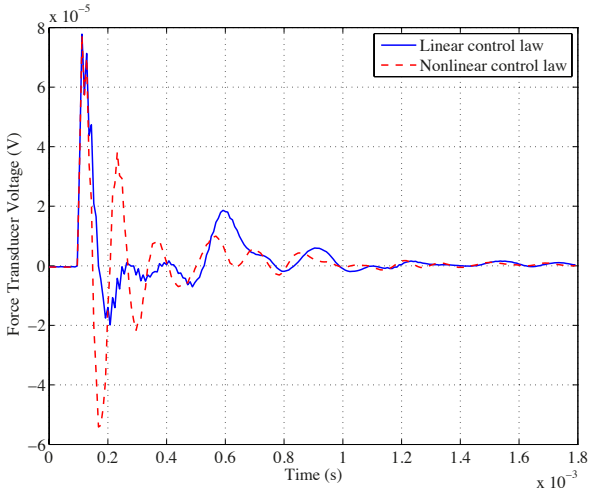

Fig. 7: Measured transducer voltage for the linear and nonlinear control law.

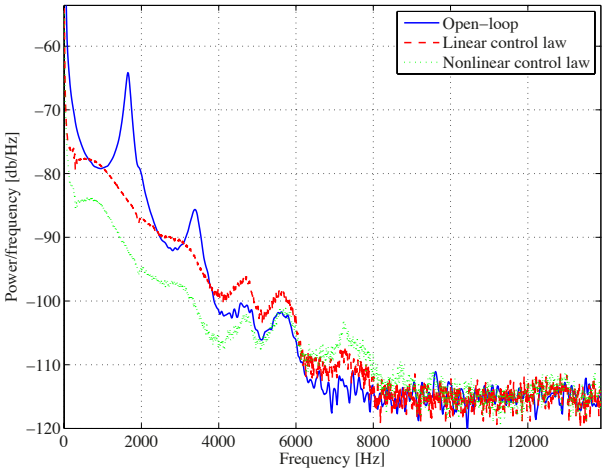

Fig. 8: Power spectral density estimate for the displacement signal when operating in open-loop, and when using the linear and the nonlinear control law.

V. Discussion

The results presented in Figs. 6 and 8 indicate that the nonlinear control law provides improved performance with regards to disturbance rejection and vibration damping over the linear control law. Fig. 6 show a reduced overshoot and a somewhat faster settling time for the nonlinear control law. It is interesting to note that the measured force is larger in the nonlinear case, indicating that the nonlinear control law produces a larger actuation signal for the same disturbance compared to the linear control law. Lastly, the power spectral density estimate in Fig. 8 confirms a significant reduction in spectral content of the displacement signal when using the nonlinear control law. As can be seen, both the linear and the nonlinear control law attenuates several resonant modes, but the nonlinear control law is apparently more effective.

VI. Conclusions

This paper presents the application of a nonlinear augmentation of the vibration damping control scheme integral force feedback (IFF). The original linear control law was compared to the augmented nonlinear control law in a set of experiments using a nanopositioning device exhibiting highly resonant vibrational modes. The nonlinear control law was seen to result in improved damping performance compared to the original linear scheme, while having the same theoretical stability properties, i.e. the augmentation retains the robust $\mathcal{L}_2$ stability property.

Appendix

The following Theorems are taken from [30], [31].

Theorem 1: The operator $\mathcal{H} : \mathcal{L}^n_{2e} \rightarrow \mathcal{L}^n_{2e}$ is strictly passive if and only if

$$\exists \beta,\ \delta > 0,\ \langle \mathcal{H}x | x \rangle_T \geq \delta \|x\|^2_T + \beta,\ \forall\, x \in \mathcal{L}^n_{2e},\ \forall\, T \in \mathcal{T}\ .$$

Typically $\mathcal{T} \in \mathbb{R}_+,\ \mathbb{R},\ \mathbb{Z},$ or $\mathbb{Z}_+$.

Theorem 2: Let $\mathcal{H} : \mathcal{L}_{2e}^1 \to \mathcal{L}_{2e}^1$ and be defined by $\mathcal{H}u \triangleq H * u$, where $H \in \mathcal{A}$ and $u \in \mathcal{L}_{2e}^1$, then

$$H \text{ is passive } \Leftrightarrow \mathbf{Re}\left[\widehat{H}(j\omega)\right] \geq 0,\ \forall\, \omega \in \mathbb{R}\ .$$

Note that since $H \in \mathcal{A}$, $\mathcal{H}$ is casual, where $\mathcal{A}$ denotes the set of generalized functions (distributions) $f(\cdot)$ such that $f(t) = 0$ when $t < 0$, and have the form

$$f(t) = \sum_{\infty}^{i=0} f_i \delta(t - t_i) + f_a(t),\ t \geq 0\ ,$$

where $\delta(\cdot)$ denotes the unit delta distribution, $0 \leq t_0 < t_1 < \ldots$ are constants, and $f_a(\cdot)$ is a measurable function.

Theorem 3: The feedback system of Fig. 9 is $\mathcal{L}_2$-stable with finite gain and zero bias if G_2 is strictly passive and has finite gain, and G_1 is passive.

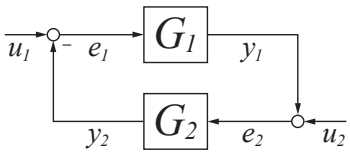

Fig. 9: General feedback system.

REFERENCES

[1] S. Devasia, E. Eleftheriou, and S. O. R. Moheimani, "A Survey of Control Issues in Nanopositioning," *Control Systems Technology, IEEE Transactions on*, vol. 15, no. 5, pp. 802–823, 2007.

[2] A. A. Tseng, S. Jou, A. Notargiacomo, and T. P. Chen, "Recent Developments in Tip-Based Nanofabrication and Its Roadmap," *Journal of Nanoscience and Nanotechnology*, vol. 8, no. 5, pp. 2167–2186, May 2008.

[3] S. M. Salapaka and M. V. Salapaka, "Scanning Probe Microscopy," *Control Systems Magazine, IEEE*, vol. 28, no. 2, pp. 65–83, 2008.

[4] M. Fuechsle, J. A. Miwa, S. Mahapatra, H. Ryu, S. Lee, O. Warschkow, L. C. L. Hollenberg, G. Klimeck, and M. Y. Simmons, "A single-atom transistor," pp. 1–5, Mar. 2012.

[5] L. Gross, F. Mohn, N. Moll, P. Liljeroth, and G. Meyer, "The Chemical Structure of a Molecule Resolved by Atomic Force Microscopy," *Science*, vol. 325, no. 5944, pp. 1110–1114, Aug. 2009.

[6] G. Binnig and D. P. E. Smith, "Single-tube three-dimensional scanner for scanning tunneling microscopy," *Review of Scientific Instruments*, vol. 57, no. 8, pp. 1688–1689, 1986.

[7] G. Schitter, P. J. Thurner, and P. K. Hansma, "Design and input-shaping control of a novel scanner for high-speed atomic force microscopy," *Mechatronics*, vol. 18, no. 5-6, pp. 282–288, 2008.

[8] J. B. C. Engelen, H. E. Rothuizen, U. Drechsler, R. Stutz, M. Despont, L. Abelmann, and M. A. Lantz, "A mass-balanced through-wafer electrostatic x/y-scanner for probe data storage," *Microelectronic Engineering*, vol. 86, no. 4-6, pp. 1230–1233, June 2009.

[9] H. Barnard, C. Randall, D. Bridges, and P. K. Hansma, "The long range voice coil atomic force microscope," *Review of Scientific Instruments*, vol. 83, no. 2, p. 023705 (4 pages), 2012.

[10] T. Tuma, W. Haeberle, H. Rothuizen, J. Lygeros, A. Pantazi, and A. Sebastian, "A high-speed electromagnetically-actuated scanner for dual-stage nanopositioning," in *6th IFAC Symposium on Mechatronic Systems, Proceedings of the*, Hangzhou, Apr. 2013, pp. 125–130.

[11] G. M. Clayton, S. Tien, K. K. Leang, Q. Zou, and S. Devasia, "A Review of Feedforward Control Approaches in Nanopositioning for High-Speed SPM," *Journal of Dynamic Systems Measurement and Control, Transactions of the ASME*, vol. 131, no. 6, p. 061101 (19 pages), 2009.

[12] J. L. Fanson and T. K. Caughey, "Positive Position Feedback-Control for Large Space Structures," *AIAA Journal*, vol. 28, no. 4, pp. 717–724, 1990.

[13] A. Preumont, J. Dufour, and C. Malekian, "Active Damping by a Local Force Feedback with Piezoelectric Actuators," *Journal of Guidance Control and Dynamics*, vol. 15, no. 2, pp. 390–395, 1992.

[14] N. W. Hagood and A. von Flotow, "Damping of Structural Vibrations with Piezoelectric Materials and Passive Electrical Networks," *Journal of Sound and Vibration*, vol. 146, no. 2, pp. 243–268, 1991.

[15] H. Pota, S. O. R. Moheimani, and M. Smith, "Resonant Controllers for Smart Structures," *Smart Materials and Structures*, vol. 11, no. 1, pp. 1–8, 2002.

[16] S. S. Aphale, A. J. Fleming, and S. O. R. Moheimani, "Integral Resonant Control of Collocated Smart Structures," *Smart Materials and Structures*, vol. 16, no. 2, pp. 439–446, 2007.

[17] S. S. Aphale, B. Bhikkaji, and S. O. R. Moheimani, "Minimizing Scanning Errors in Piezoelectric Stack-Actuated Nanopositioning Platforms," *Nanotechnology, IEEE Transactions on*, vol. 7, no. 1, pp. 79–90, 2008.

[18] A. J. Fleming, "Nanopositioning System With Force Feedback for High-Performance Tracking and Vibration Control," *Mechatronics, IEEE/ASME Transactions on*, vol. 15, no. 3, pp. 433–447, 2010.

[19] M. W. Fairbairn, S. O. R. Moheimani, and A. J. Fleming, "Q Control of an Atomic Force Microscope Microcantilever: A Sensorless Approach," *Microelectromechanical Systems, Journal of*, vol. 20, no. 6, pp. 1372–1381, 2011.

[20] A. A. Eielsen and A. J. Fleming, "Passive Shunt Damping of a Piezoelectric Stack Nanopositioner," in *American Control Conference, Proceedings of the*, Baltimore, MD, 2010, pp. 4963–4968.

[21] B. Bhikkaji and S. O. R. Moheimani, "Integral Resonant Control of a Piezoelectric Tube Actuator for Fast Nanoscale Positioning," *Mechatronics, IEEE/ASME Transactions on*, vol. 13, no. 5, pp. 530–537, 2008.

[22] S. Boyd and C. Barratt, *Linear Controller Design: Limits of Performance*. Prentice-Hall, 1991.

[23] R. K. Kanestrøm and O. Egeland, "Nonlinear Active Vibration Damping," *Automatic Control, IEEE Transactions on*, vol. 39, no. 9, pp. 1925–1928, 1994.

[24] B. M. B. Brogliato, R. Lozano and O. Egeland, *Dissipative Systems Analysis and Control*, 2nd ed. Springer, 2006.

[25] K. K. Leang and A. J. Fleming, "High-Speed Serial-Kinematic SPM Scanner: Design and Drive Considerations," *Asian Journal of Control*, vol. 11, no. 2, pp. 144–153, 2009.

[26] A. Preumont, *Mechatronics*. Springer, 2006.

[27] ——, *Vibration Control of Active Structures: An Introduction*, 2nd ed. Kluwer Academic Publishers, 2002.

[28] A. Preumont, B. de Marneffe, A. Deraemaeker, and F. Bossens, "The damping of a truss structure with a piezoelectric transducer," *Computers & Structures*, vol. 86, no. 3-5, pp. 227–239, Feb. 2008.

[29] G. C. Goodwin, S. F. Graebe, and M. E. Salgado, *Control System Design*. Prentice Hall, 2000.

[30] M. Vidyasagar, *Nonlinear Systems Analysis*, 2nd ed. Prentice Hall, Inc, 1993.

[31] A. C. Desoer and M. Vidyasagar, *Feedback Systems: Input Output Properties*. Academic Press Inc, 1975.